REVIEW ARTICLES
PUBLISHED ONLINE: 25 SEPTEMBER 2017 | DOI: 10.1038/NPHYS4274
nature physics

Emergent functions of quantum materials

Yoshinori Tokura[1,2]*, Masashi Kawasaki[1,2] and Naoto Nagaosa[1,2]

Materials can harbour quantum many-body systems, most typically in the form of strongly correlated electrons in solids, that lead to novel and remarkable functions thanks to emergence—collective behaviours that arise from strong interactions among the elements. These include the Mott transition, high-temperature superconductivity, topological superconductivity, colossal magnetoresistance, giant magnetoelectric effect, and topological insulators. These phenomena will probably be crucial for developing the next-generation quantum technologies that will meet the urgent technological demands for achieving a sustainable and safe society. Dissipationless electronics using topological currents and quantum spins, energy harvesting such as photovoltaics and thermoelectrics, and secure quantum computing and communication are the three major fields of applications working towards this goal. Here, we review the basic principles and the current status of the emergent phenomena and functions in materials from the viewpoint of strong correlation and topology.

Emergence is a concept developed for many-body systems, indicating the properties, phenomena, and functions that never appear in the individual elements but are realized only when a huge number of elements get together[1]. Inside materials, emergent phenomena are often seen due to the interaction of electronic states; with recent developments on electronic states in solids schematically summarized in Fig. 1a. Electrons in solids have several degrees of freedom: charge, spin and orbital, and are characterized by the topological nature determined by the atomic potential on the crystal lattice structure, as schematically shown in Fig. 1b. These five attributes are coupled together and determine the overall responses to stimuli, which appear as materials' electrical, magnetic, optical, thermal, and mechanical properties.

These collective electrons demonstrate various macroscopic quantum phenomena, the representative example of which is superconductivity. One of the big challenges in condensed matter physics is to increase the temperature (T_c) at which superconductivity can be observed to above room temperature. However, there are many other macroscopic quantum phenomena that are already observable above room temperature. One is magnetism (by the Bohr–van Leeuwen theorem), and the other is ferroelectricity[2,3]. Remarkably, there are common features of these three macroscopic quantum phenomena: the order parameter, which is of quantum origin, behaves as a classical quantity, and the quantum topology plays a crucial role.

The topological nature of the electronic states is the key concept in the most recent developments in understanding quantum materials. The quantum Hall effect, topological insulators, and topological superconductors are all characterized by nontrivial topologies in Hilbert space. The Berry phase, which describes the connection and curvature of the subspace of Hilbert space, plays the central role in the unified principle to describe this topological nature[4]. Relativistic effects and consequent spin–orbit interactions are deeply connected to the Berry phase. They are also key to spintronics applications, where the electrical manipulation of spins is being pursued.

Topology, along with strong correlations—which are due to the strong Coulomb repulsion among electrons—are two major streams of condensed matter physics, and they are now merging, creating new concepts, phenomena, and also functions. So how will these astonishing properties of quantum materials be utilized in applications? The desired functions for quantum materials are: ultralow energy consumption to cope with the impending energy crisis; high speed and huge capacity to cope with an advanced information society; high security; and environmentally benign properties. The basic idea to realize and meet these requirements is quantum emergence. Here, we discuss the dissipationless topological currents, including displacement current, spin current, and edge/surface currents in quantum materials, that may enable a novel state variable for future memory and logic technologies with minimal energy dissipation.

Mottronics

The metal–insulator transition (MIT) in solids is one of the most important features in quantum materials. Origins of the MIT are versatile, including simple bandgap closing, Anderson localization, and polaron self-trapping driven by electron–lattice interactions, but many are related to electron–electron interaction beyond the one-particle picture—generally called the Mott transition[5,6]. At a finite temperature, preferably around and beyond room temperature, the MIT can provide useful functions, enabling gigantic, ultrafast switching of versatile physical properties, not only electrical conductivity but also other transport, magnetic and optical properties. The terminology 'Mottronics' was coined to represent the concept of electron technology exploiting the Mott transition.

In general, the Mott transition can be classified into two types[6]; bandwidth control of the MIT, which changes the effective electron correlation strength represented by the ratio of the electron correlation energy U to the one-electron bandwidth W; and band-filling control, which changes the integer (or rational) electron number n per atom site (for example, half-filling state; $n = 1$) by chemical or electrostatic doping. Bandwidth-control and filling-control MITs are typically observed in a family of perovskites (AMO_3) and pyrochlores ($A_2M_2O_7$) (M = transition metal), in which the A-site ionic size can control W via the change of the O–M–O bond angle, and the mixed ionic valences in the A site can change the band filling[5]. The bandwidth-control MIT on these correlated electron systems often spans a wide temperature range

[1]RIKEN Center for Emergent Matter Science (CEMS), Wako, Saitama 351-0198, Japan. [2]Department of Applied Physics and Quantum Phase Electronics Center (QPEC), University of Tokyo, Bunkyo-ku, Tokyo 113-8656, Japan. *e-mail: tokura@riken.jp

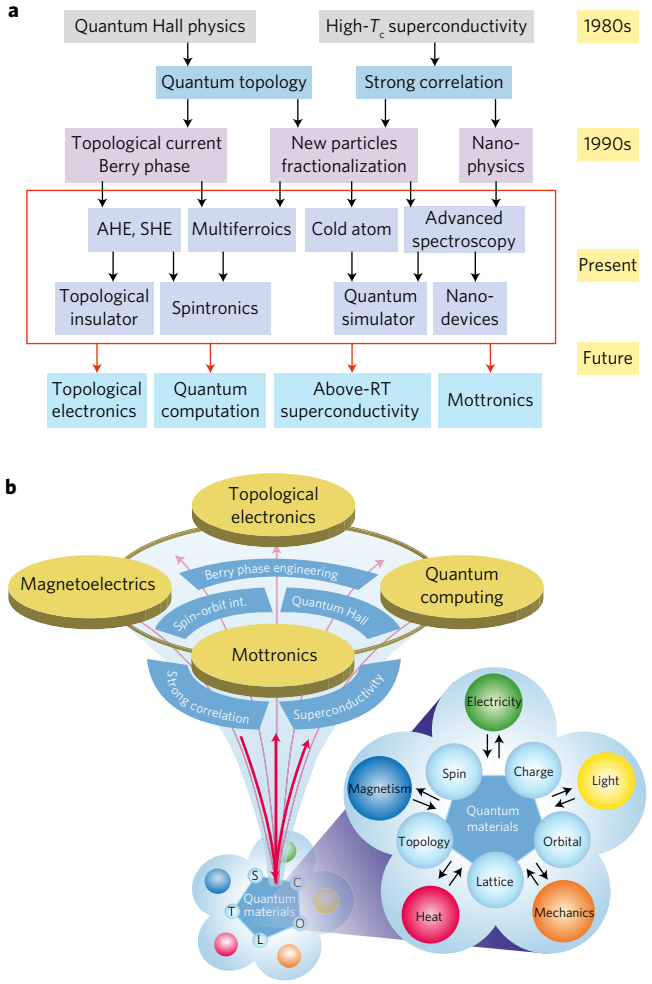

Figure 1 | Concepts in quantum materials. a, Brief history of the research on physics of quantum materials and functions. **b**, The bottom pentagon shows various degrees of freedom of strongly correlated electrons in solids, which respond to external stimuli. These strong couplings lead to the emergent functions with the cross correlations among different physical observables and to developments towards the applications of emergent functions such as Mottronics, magnetoelectrics, topological electronics, and quantum computing, each of which is discussed in this article.

from zero to above room temperature, reflecting the large energy scale of the competing W and U.

Among them, the simple but most conspicuous example for the band-filling-control MIT is the case of copper-oxide superconductors, where a quasi-two-dimensional electronic structure with half filling (one hole per Cu) forms the parent correlated insulator composed of CuO_2 square-lattice sheets and sandwiching ionic block layers as the charge reservoir[6]. Hole or electron doping—the procedures used to represent the reduction or increment of electron band filling—is possible via the partial substation of the block layers with different-valence cations or a change of the oxygen content, which drives the system to a metallic or high-temperature superconducting state, viewed as a 'doped Mott insulator'[7].

Needless to say, the exploration of higher- or room-temperature (RT) superconductors is of tremendous importance for practical applications, from lossless power cables to electrical apparatus such as superconducting magnets, motors, and information appliances such as microwave filters. The current state of the art for the highest-temperature zero-resistance superconducting state is around 153 K for Hg-based cuprate superconductors under high pressures above 10 GPa (refs 8,9), and around 190 K for H_3S under a very high pressure of 200 GPa (ref. 10). As for the present status of applications of high-temperature superconductors, benchmark examination towards large-scale application are in progress. For dissipationless energy transfer, long cables such as Bi-based cuprates sheathed in Ag and Y–Ba–Cu–O coated conductors are being examined for power transfer[11,12]. As for electronics, highly sensitive magnetic-field sensors employing SQUID (superconducting quantum interference device) are actually already used for the non-destructive inspection of infrastructure and searching for underground minerals[13].

An electron in a correlated system has three attributes: charge, spin and orbital (Fig. 1b). The spin, charge, and orbital degrees of freedom and their coupled dynamics can produce versatile electronic phases as well as possible electronic phase separation and pattern formation; all of these features play important roles in the MIT, particularly for d-electron compounds. Not only the half band filling but also the fractional case lead to an insulating ground state accompanying the regular ordering of localized charge, termed charge ordering; the state frequently accompanies the ordering also in spin and orbital sectors[14] as in the undoped system. Upon external stimulation, such as by chemical doping, electrostatic doping, pressure application or photo-excitation, the MIT can be exploited as a function, exemplifying the cross-correlation among the electric, magnetic, mechanical, and photonic inputs and outputs, as shown in Fig. 1b. Figure 2 shows some examples of the controlled MIT.

The colossal magnetoresistance (CMR) manganites[15] provide a good arena to test exotic phase-control functions; Fig. 2a shows typical CMR phenomena, viewed as a magnetic-field-induced MIT[16]. The external magnetic field works on the spin sector so as to align the spin moment (towards the ferromagnetic state), and eventually this strongly spin–charge–orbital coupled system undergoes a collective transition to a ferromagnetic metallic state, accompanying the melting of charge/orbital order or their short-range order. Likewise, photo-excitation works on the charge/orbital sector, enabling photo-melting of the spin–charge–orbital coupled order and induces a ferromagnetic metallic state[17], as shown in Fig. 2c.

Among the possible MIT functions, electrical control is the most useful for Mottronics. Figure 2b exemplifies the electric-double-layer transistor (EDLT) gate control of the MIT in VO_2 films[18]; a clear MIT is observed upon gating, ascribed to the filling-control Mott transition, although its doping mechanism is still controversial[18,19]. As shown in the upper panel of Fig. 2b, this gating-induced MIT accompanies a large change of the infrared spectra, again demonstrating the potential application to radiation devices, like a dimming window[20].

The application of such MIT in integrated circuits is very attractive for non-volatile memories called Resistance Random Access Memory (ReRAM), where information is memorized as metallic or insulating states of a device cell in a non-volatile and rewritable manner. Expected advantages of ReRAM compared with flash memory include higher-density integration, higher speed, and lower energy consumption[21,22]. The MIT actually taking place in such memory devices may be different from what is observed for bulk materials. Tiny changes in the electronic structure or band filling at electrode/oxide interfaces can change the total resistance of memory cells by decades[23]. The process of electrical injection/rejection of oxygen ions, which should induce a change in the band filling, is considered to be one of the plausible origins of the gigantic electrical resistance switching widely observed for transition-metal oxides, including the example of the CMR manganite, which is still at the early stages of research[24]. The ReRAM has been industrialized as a storage-class memory that is between high-speed and low-density DRAM (Dynamic RAM) and low-speed and high-density storage such as hard disc drives or solid-state drives based on flash memory.

In addition to these quasi-steady state functions, non-equilibrium Mott physics, which is experimentally explored by a pump-and-probe technique, provides one other research direction

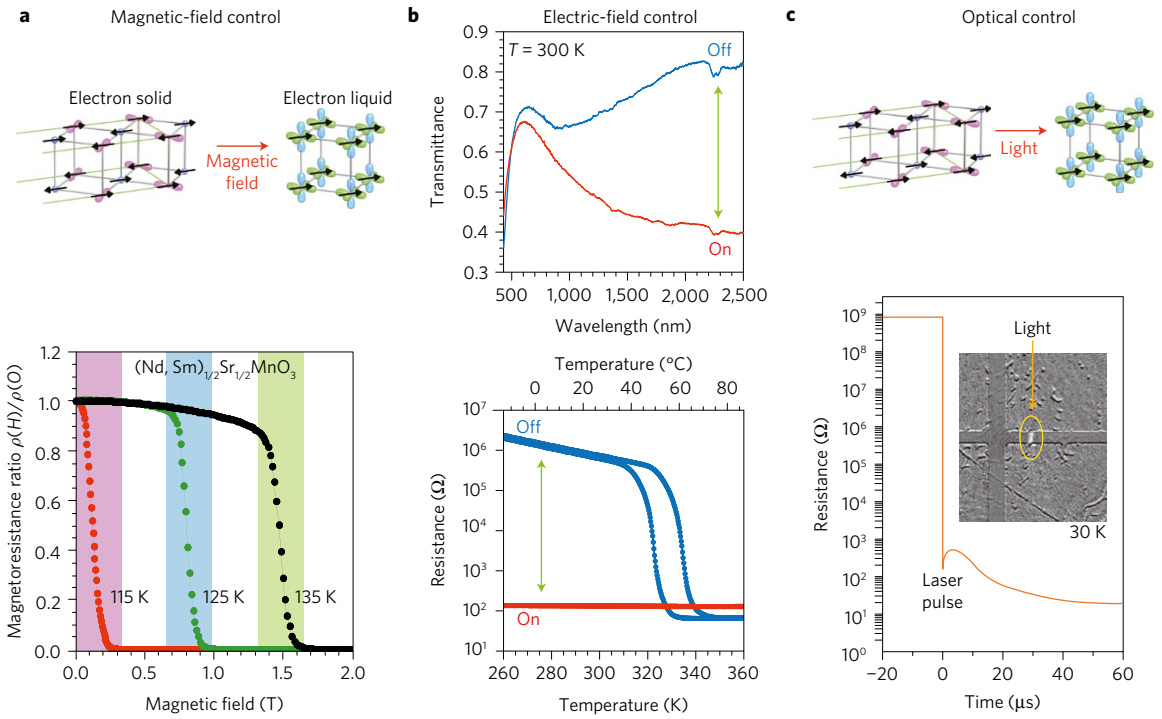

Figure 2 | Electronic phase control of correlated-electron materials. a, Colossal magnetoresistance (CMR) in the perovskite manganite. The upper panel schematically represents the magnetic-field-induced melting of the charge-orbital ordered state as the microscopic origin of CMR. **b**, Electric-double-layer (EDL) gating-induced insulator–metal transition in VO_2 thin film. The upper panel shows the concurrent switching of the near-infrared photo-absorption spectrum, representing radiation device functionality. **c**, Photo-melting of the charge-orbital ordered state in manganite. Adapted from ref. 16, AAAS (**a**); ref. 20, AIP (**b**, top); ref. 18, Macmillan Publishers Ltd (**b**, bottom); and ref. 17, AAAS (**c**).

for the functionality of correlated quantum materials. An ultrafast (typically femtosecond to picosecond) excitation with a laser pulse or electron beam may cause a transient phase conversion/promotion through electron–electron and/or electron–lattice interactions at the excited state, providing ultrafast control of the electronic state[25]. One of the most amazing phenomena reported recently is the transient photo-creation of possible room-temperature superconductivity in cuprate and C_{60}-based superconductors[26,27].

Magnetoelectrics

Electric polarization and magnetism in solids are both quantum mechanical in nature. Mutual control of electricity and magnetism has long been sought after among quantum materials, and would provide versatile functions. Symmetry analysis predicts the presence of a linear magnetoelectric (ME) effect—namely the polarization P proportional to the applied magnetic field (H) or the magnetization M proportional to the applied electric field (E)—in the system (termed here magnetoelectrics) where both time-reversal and space-inversion symmetries are broken. A classic example is Cr_2O_3, in which the linear ME effect was first conjectured[28] and experimentally verified[29]. The ME tensor α_{ij} (in a form that $M_i = \alpha_{ij}E_j$) in its antiferromagnetically ordered phase has diagonal components ($\alpha_{11} = \alpha_{22}$ and α_{33}, here suffix 3 indicates the component along the c-axis, with suffix 1, 2 perpendicular to c), which originate from the spin–orbit interaction and/or the exchange striction mechanism (see below). While Cr_2O_3 is a non-polar spin-collinear antiferromagnet, polar ferromagnets (or polar ferrimagnets) straightforwardly fulfil the requirement of magnetoelectrics endowed with the linear ME effect; therein the $E(H)$-field-induced magnetization M (polarization P) shows up as an addition to the spontaneous $M(P)$. This was nicely exemplified by the polar ferrimagnet $Ga_{1-x}Fe_{1+x}O_3$ (refs 30,31), and more recently by $(Fe_{1-x}Zn_x)_2Mo_3O_8$ (ref. 32). Nevertheless, the d.c. linear ME effect observed has remained far smaller than the level required for any practical application.

To explore possible application of magnetoelectrics, it is indispensable to enhance the ME effect by two orders of magnitude; this can partially be achieved with the dynamical (optical) ME effect, which uses electronic or magnetic resonances (see below). For the d.c. or low-frequency ME effect, on the other hand, one promising route is to exploit the gigantic response upon the magnetoelectric phase transition in multiferroics[33]. The terminology multiferroics represents the materials where plural ferroic orders such as ferroelectricity (with spontaneous polarization P) and ferromagnetism (with spontaneous magnetization M) are present. In a little broader context, it represents materials with both ferroelectric and magnetic orders, such as antiferromagnetic, ferrimagnetic or helimagnetic ones—systems with an order parameter of magnetization M_Q with an arbitrary wavevector Q. In multiferroics, the coexistent M and P may respond to relatively weak H and E, respectively, mostly via the field-induced motion of the respective and/or composite domain walls. When the mutual coupling between M and P is strong enough, a gigantic ME effect should be possible—with H-control of the spontaneous (ferroic) P as well as E-control of the ferroic M. The issue is how to design and realize multiferroic materials with such a strong M–P coupling[34].

In this context, Khomskii[35] classified multiferroics into two types: type-I, where ferroelectricity and magnetism are of distinct origins; and type-II, with magnetic-order-driven ferroelectricity. The former group includes $BiFeO_3$ (ref. 36) and hexagonal $YMnO_3$ (refs 37,38), which show relatively large spontaneous polarization and high ferroelectric/magnetic transition temperatures, albeit with weak coupling between polarization and magnetism. By contrast, type-II multiferroics inherently host strong ME coupling despite smaller ferroelectric polarization and lower transition temperature[38]. Various types of spin orders can produce ferroelectric P. Three representative mechanisms for spin-order-induced ferroelectricity[39,40] are shown in the upper panel of Fig. 3: symmetric spin exchange interaction $\mathbf{e}_{ij}(\mathbf{S}_i \cdot \mathbf{S}_j)$, antisymmetric spin exchange interaction

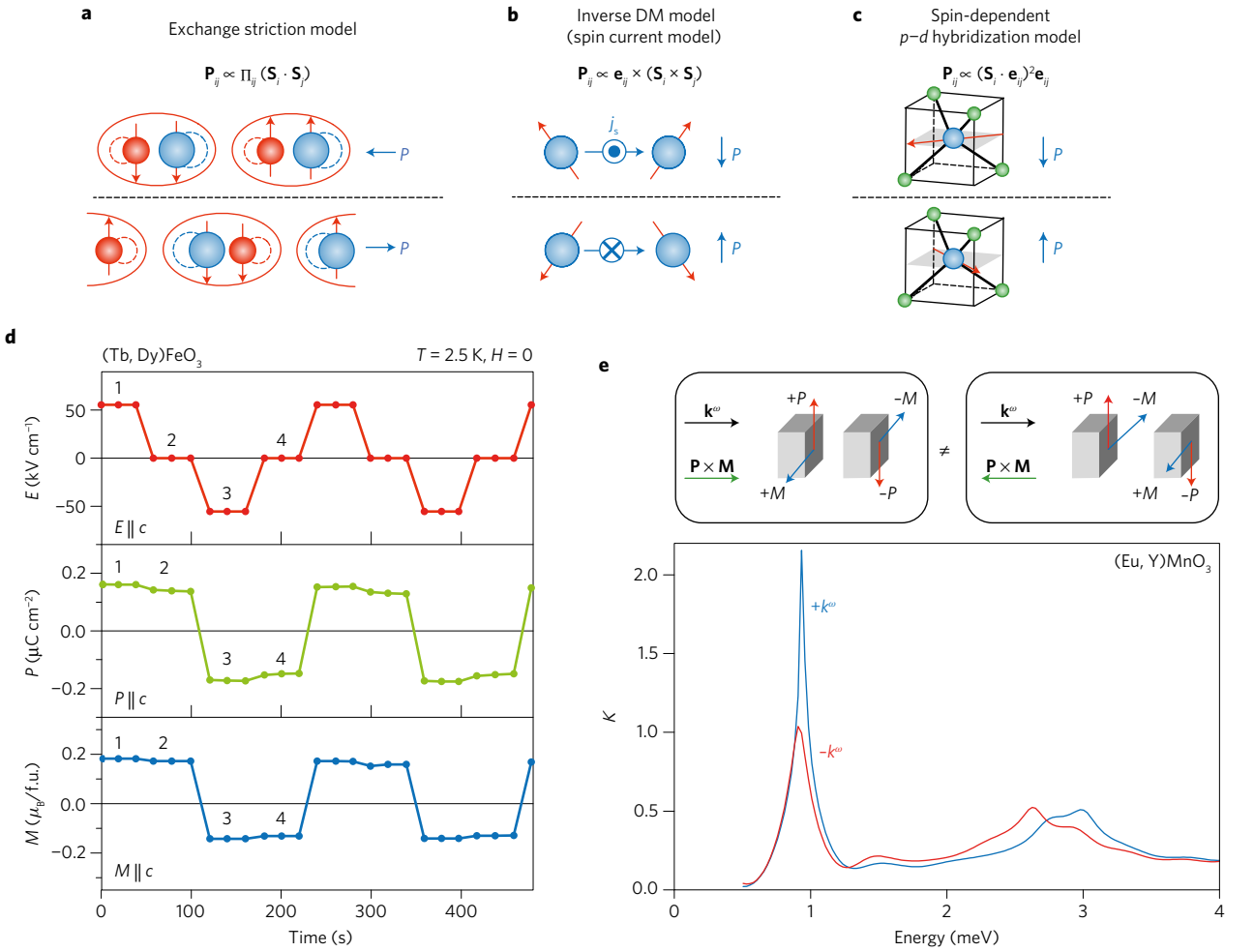

Figure 3 | Multiferroics of spin origin and their magnetoelectric responses. a–c, The respective models for multiferroic mechanism; exchange striction model (**a**) , inverse Dzyaloshinskii–Moriya model or spin-current model (**b**) , and spin-dependent *p–d* hybridization model (**c**). $\mathbf{P}_{ij}$ stands for the local polarization occurring on the bond between the *i*th and *j*th sites. $\mathbf{S}_i$ ($\mathbf{S}_j$) represents the spin on the *i*th (*j*th) site, and $\mathbf{e}_{ij}$ the unit vector connecting the *i*th and *j*th sites. **d**, Electric-field switching of the spontaneous magnetization (**M**) upon the reversal of polarization (**P**) in perovskite ferrites (Tb,Dy)FeO_3 based on the exchange striction mechanism. **e**, Electromagnon resonance (electrically active magnetic resonance) spectra for perovskite manganite (Eu,Y)MnO_3, showing the optical magnetoelectric effect—that is, directional dichroism with respect to oppositely propagating, $+\mathbf{k}^{\omega}$ versus $-\mathbf{k}^{\omega}$, terahertz light beams. Reproduced from ref. 39, IOP (**a–c**); and ref. 42, Macmillan Publishers Ltd (**d**). Adapted from ref. 46, APS (**e**).

$\mathbf{e}_{ij} \times (\mathbf{S}_i \times \mathbf{S}_j)$, and spin–ligand interaction (spin-dependent *p–d* hybridization) $(\mathbf{e}_{il} \cdot \mathbf{S}_i)^2 \mathbf{e}_{il}$. These models have recently led the development or rediscovery of an increasing number of multiferroics[39]. Among them, the symmetric exchange interaction working between the neighbouring spins, $\mathbf{S}_i$ and $\mathbf{S}_j$, may induce polar striction along the bond direction $\mathbf{e}_{ij}$, as shown in Fig. 3a. Orthoferrites with distorted ($GdFeO_3$ type; P_{bnm}) perovskite structure, $RFeO_3$ (R = Gd, Tb, Dy and their solid solutions)[41,42] can be one such example at low temperatures, for example, $T < 4$ K. Therein, the exchange interaction between the R 4*f* moment and the Fe 3*d* spin plays a key role in striction-induced ferroelectricity. Figure 3d shows the pulsed E-field effect on the magnetization for the ferromagnetic–ferroelectric phase of $RFeO_3$ ($R = Dy_{0.7}Tb_{0.3}$), in which the weak ferromagnetism arises from the Dzyaloshinskii–Moriya (DM) interaction in the distorted perovskite lattice[42]. When the E field is changed in a step-like manner, M is perfectly reversed upon the reversal of P in a non-volatile manner. This E-control of the ferromagnetic moment is capable only at low temperatures due to the use of R 4*f* moment order and hence not meaningful for immediate application. However, it would give a hint to the development of the E-control reversal of M, which would constitute a dissipationless memory device if it were realized beyond room temperature.

Another important class of type-II multiferroics is based on the antisymmetric spin exchange mechanism (Fig. 3b), termed the spin-current model or inverse DM model. By use of the inherent strong M-P coupling based on this mechanism, the $H(E)$-induced change of P (M) is ubiquitously observed for cycloidal or transverse-conical spin multiferroics. From the viewpoint of applications, this E-induced reversal of the ferromagnetic M is the most important effect, yet the hitherto developed multiferroics still suffer from difficulties due to the weakness of the spin-induced P and/or to the leaky loss current under high voltage. Nevertheless, some hexaferrite compounds with above-room-temperature conical spin states show promise towards room-temperature operation[43,44].

One of the most important functions related to E-controlled magnetism[45] is the dynamical ME response. The (linear) ME susceptibility α_{ij} can be extended to the a.c. or optical frequency region, such that $P_i(\omega) = \alpha_{ij}(\omega)H_j(\omega)$ and $M_i(\omega) = {}^t\alpha_{ij}(\omega)E_j(\omega)$. In multiferroics, or more broadly in magnetoelectrics, $\alpha_{ij}(\omega)$ shows resonance structures at ME excitations. In the case of spin waves or magnons, such an excitation can be electrically (electric dipole) active and hence called an electromagnon. The relation between $\mathbf{E}(\omega)$ and $\mathbf{H}(\omega)$ obeys the wave equation as derived from the Maxwell equations. Therefore, the presence of the dynamical ME

effect adds an additional term ($\pm\alpha$) to the optical response (complex refractive index) that is dependent on the sign (direction) of the light wavevector. This kind of optical ME effect is termed directional dichroism. Figure 3e exemplifies the spectra of the imaginary part of the refractive index (absorption spectra) for the electromagnon modes in perovskite type $R\mathrm{MnO_3}$ (here $R = \mathrm{Eu_{0.5}Y_{0.5}}$) with different light propagation directions ($\pm k^{\omega}$) (ref. 46). The lower-lying sharp peak at 1 meV represents the spin-current electromagnon mode[47], while the higher-lying broad peak is assigned to the E^{ω}-active but H^{ω}-inactive magnon (located at the magnetic zone edge); the latter was the first-reported electromagnon for $R\mathrm{MnO_3}$ (ref. 48). A large directional dichroism of up to ∼50% has been observed for the lower-lying electromagnon modes with spin-current origin. Like this case, the ferroelectric cycloidal magnets can universally host gigantic directional dichroism, especially through the electromagnon resonance mode associated with the rotation of the spin-spiral plane. Conical magnets can be found ubiquitously, even at room temperature, particularly in the family of hexaferrites[49,50], in which the electromagnons may enable fast electrical control of the magnetic structure to be realized. Similar gigantic directional dichroism has recently also been observed in other multiferroics based on the spin-dependent d–p hybridization mechanism (Fig. 3c) via the electromagnon[51] as well as the electronic d–d excitation[52].

Berry phase engineering

In 1984, M. V. Berry[4] considered the adiabatic process where the wavefunction is confined within a manifold of Hilbert space, which is characterized by the connection acting as the vector potential[53]. This vector potential gives a generalized 'emergent electromagnetic field'. This is an essential concept to describe the topological properties of condensed matter (Fig. 1b), and therefore the engineering of the Berry phase is key for designing emergent functions of quantum materials.

An example of Berry phase is shown in Fig. 4a. Suppose we have three spins 1, 2 and 3, which are coupled to the conduction electron. The electron moving around this triangle will get a phase factor which is 1/2 of the solid angle subtended by these three spins, called scalar spin chirality[54]—the Aharonov–Bohm effect due to an emergent magnetic field. For ferromagnetic spins on a tetrahedron (a unit of pyrocholore lattice), a strong magnetic anisotropy enforces a non-coplanar spin structure, as shown in Fig. Fig. 4b, which results in the Hall effect, as shown in Fig. 4d[55,56]. Note that the emergent magnetic field becomes very strong—on the order of ∼4,000 T for a spin texture of ∼1 nm size.

Skyrmions are another example with scalar spin chirality, whose solid angle, as schematically shown in Fig. 4c, is characterized by the topological number $N_{\mathrm{sk}} = 1/(4\pi)\iint \mathrm{d}^2\mathbf{r}\,\mathbf{n}\cdot((\partial\mathbf{n}/\partial x)\times(\partial\mathbf{n}/\partial y))$, which counts how many times the direction of the spin $\mathbf{n}(r) = \mathbf{n}(x,y)$ wraps the unit sphere[57]. This topological index gives skyrmions stability against dissociation. The solid angle also gives rise to a Hall effect in materials with a metastabilized skyrmion crystal phase[58], which is known as the topological Hall effect (THE), shown in Fig. 4e.

Electromagnetic induction of emergent electromagnetic fields has also been demonstrated by looking at the current-dependent Hall response[59]. Once the considerations above are extended to three dimensions, one can define another topological spin texture called an emergent magnetic monopole[60–62], which can act as a source or sink of a skyrmion string in three dimensions.

One can also consider the Berry phase connection in momentum ($\mathbf{k}$)-space, which has the physical meaning of an intracell coordinate, with the position of a particle given by[63]

$$r_{\alpha} = i\frac{\partial}{\partial k_{\alpha}} + a_{\alpha}(\mathbf{k}) \qquad (1)$$

Furthermore, this leads to the additional (anomalous) velocity to the particle, and results in topological currents, which are the source of many intriguing phenomena, such as ferroelectricity[2,3], the quantum Hall effect[64,65], the anomalous Hall effect[54], and the intrinsic spin Hall effect[66]. Topological currents are essentially dissipationless since they do not require a deviation of the electron distribution function in momentum space. The integral of the emergent magnetic field over the first Brillouin zone is also quantized, which is related to the Hall conductance[67]. Furthermore, it opens a new way to characterize the electronic states in solids from the viewpoint of topological order, in sharp contrast to the conventional order associated with symmetries.

An important issue is how to design Berry phases to enhance topological currents. The degeneracy of energy dispersions gives a clue to this question. When at least one of time-reversal T and spatial inversion I symmetries are broken, the Kramer's degeneracy is lifted at generic k-points, and the band crossings are described by 2×2 matrices—Weyl fermions. In Fig. 5a the band crossing occurs at $\mathbf{k} = \mathbf{k}_0$, which gives a diverging emergent magnetic field and acts as a magnetic monopole[68]. Physical consequences of Weyl fermions have been discussed in the context of the anomalous Hall effect[68] and magnon dynamics[69] in the itinerant ferromagnet $\mathrm{SrRuO_3}$, as shown in Fig. 5b.

In certain materials, these Weyl fermions exist exactly at the Fermi energy, which determines the low-energy transport properties of the system. This class of materials is called Weyl semimetals and many three-dimensional Weyl semimetals have been predicted theoretically and confirmed experimentally[70]—graphene is a two-dimensional version[71]. There are always an equal number of Weyl fermions with positive and negative chiralities in the band structure[72]. There must also be a surface state that connects them, known as a Fermi arc[73]. And an effect known as the chiral anomaly, discussed for both Weyl and Dirac fermions[74], which results in a negative magnetoresistance, was theoretically predicted[75] and observed experimentally[76].

One direction for future developments is to generalize the Berry phase into a matrix form, such as a non-Abelian group SU(2) matrix in the spin space of a Kramers doublet, which can be finite even in the presence of both spatial inversion (I) and time-reversal (T) symmetries. With a relativistic spin–orbit interaction, this leads to the intrinsic spin Hall effect[66], the quantized version of which has led to the discovery of topological insulators, described in the next section. Another extension is to consider the Berry phase for neutral particles, such as photons[77,78] and magnons[79–81].

The generalization of the Berry phase idea to non-equilibrium states is a recent focus related to the shift current, with possible application to photovoltaics[82–86]. When steady transitions occur from the valence to conduction bands, as shown in Fig. 5c, the continuous shift of electrons results in a d.c. current called a shift current, as expected from the change in $a_{\alpha}(\mathbf{k})$ in equation (1). Note that this is possible when either time-reversal (T) or spatial inversion (I) symmetries are broken. A first-principles band structure calculation in $\mathrm{BaTiO_3}$ shows a strong dependence of the shift current on the incident photon energy, as shown in Fig. 5d[87], in good agreement with experiment. This mechanism might also be relevant for ferroelectric-like photovoltaic materials, where the high-efficiency photovoltaic action is reported[88].

To design Berry phases, detailed first-principles calculations provide a powerful tool[54]. The band crossings in momentum space and nano-scale spin textures in real space are the two basic principles to enhance Berry phases. Artificial structures such as interfaces and superstructures will help here[89]. Especially as inversion symmetry (I) breaking, relevant to the Berry phase, can be controlled by the structure or gate voltages. From this viewpoint, an interesting proposal is valleytronics[90] in graphene and transition-metal dichalcogenides.

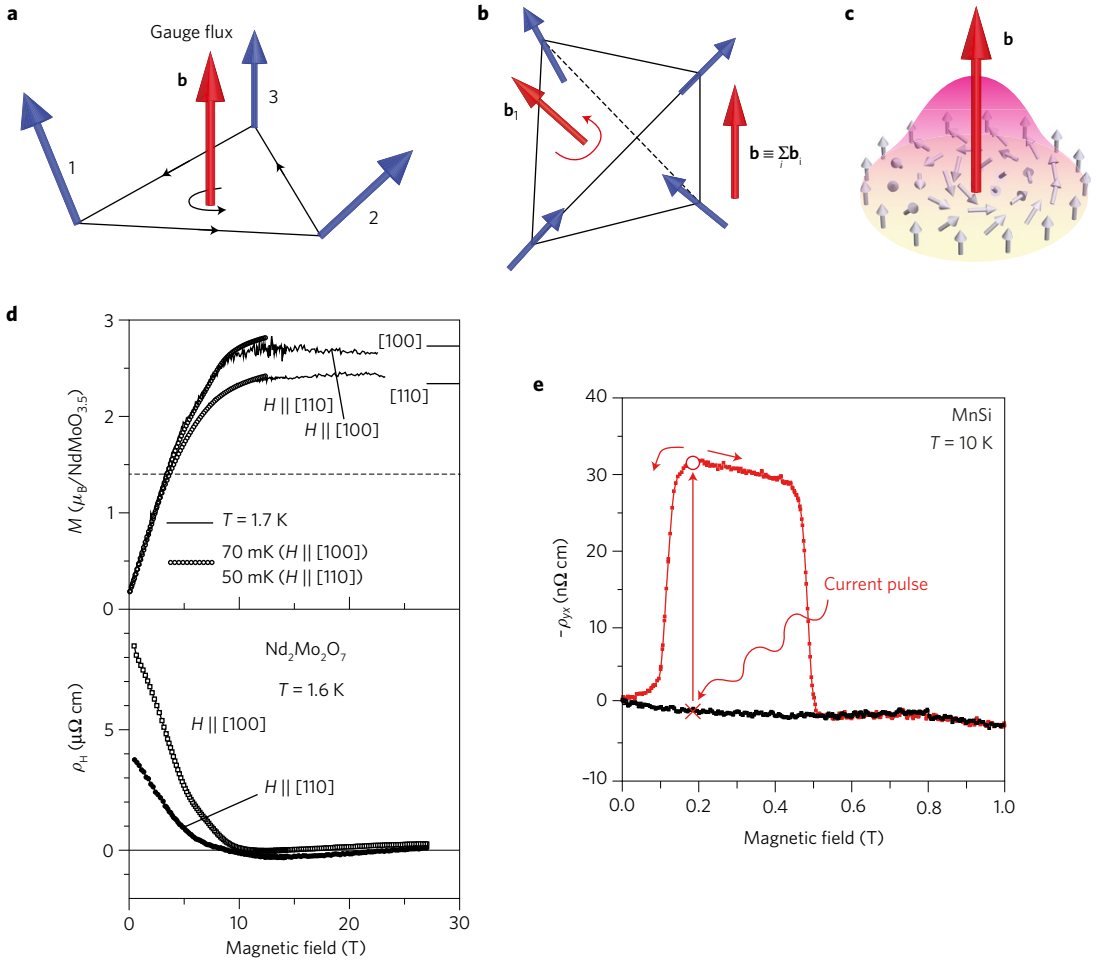

Figure 4 | Emergent magnetic field associated with the non-collinear spin configuration and its consequent physical phenomenon. a, The solid angle subtended by the three spins—that is, scalar spin chirality—acts as the emergent magnetic flux. **b**, The spins on a tetrahedron, a unit of the pyrocholore lattice, with the strong single spin anisotropy resulting in the solid angle. **c**, The emergent magnetic field accompanied by a skyrmion. **d**, The anomalous Hall effect from the scalar spin chirality in $Nd_2Mo_2O_7$. **e**, Topological Hall effect (red curve) in MnSi appearing in the metastabilized skyrmion crystal phase in comparison with the Hall resistance of the non-topological helimagnetic phase (black curve). Adapted from ref. 56, APS (**d**). Reproduced from ref. 58, Macmillan Publishers Ltd (**e**).

Topological currents driven by Berry phases are the most important concept here, which are related to the interference pattern of the phase, and essentially dissipationless. The Berry phase is nonzero even for neutral particles such as photons, magnons and phonons, as described above. Therefore, this concept will be useful in a wide range of technologies, including ferroelectrics, magnetoelectrics, spintronics, photonics, phononics and magnonics. Particularly as it provides the basis for topological electronics, discussed in the next section.

Topological electronics

The global topology of electronic states is characterized by an integer. In the case of the quantum Hall effect, this is known as the Chern number[64,65,91], but this idea can be generalized to other systems such as topological insulators and superconductors[92–95]. As a general rule, when bulk states are topologically nontrivial, there must be a robust gapless state at the surface—this is called bulk-edge correspondence. On the edge of two-dimensional quantum Hall systems, one-dimensional chiral edge channels appear due to this bulk-edge correspondence[96]. As dissipation occurs during backward scattering, which is forbidden for chiral edge modes, the edges have dissipationless transport.

At the surface of a three-dimensional topological insulator, a gapless surface state described by the two-dimensional 2 × 2 Weyl fermion appears. As spin–momentum locking (Fig. 6a) is very robust in these states, with a high energy scale, they are very promising for spintronic functions that could operate at room temperature, such as spin-current generators and charge-to-spin convertors. When topological insulators are excited with circularly polarized light, for example, electrons with only one of the spins are excited. This causes an imbalance in spin population, giving rise to a spontaneous current flow that is enhanced when E_F is within the bulk bandgap even at room temperature, as shown in the upper panel of Fig. 6d[97,98]. Conversely, when a d.c. current is fed on the surface state, the Fermi circle shifts in momentum space due to the electric field, resulting in a spin accumulation—the Rashba–Edelstein effect[99,100]—which can give rise to a spin current in an adjacent layer. The charge-to-spin conversion efficiency (q_{ICS}) in Fig. 6d is defined as the ratio of the spin-current density across the interface to the charge current density along the interface[101]. A large q_{ICS} is observed as long as E_F is located within the bulk bandgap, as seen in Fig. 6d, although a sharp dip is discerned right at the Weyl point, where the density of states is reduced. Although these experiments were done at 10 K, this type of spin-current generator should also work at room temperature.

If a topological insulator also has a perpendicular magnetization, a gap opens at the Weyl point, and the system should exhibit the quantum anomalous Hall effect (QAHE) under zero magnetic

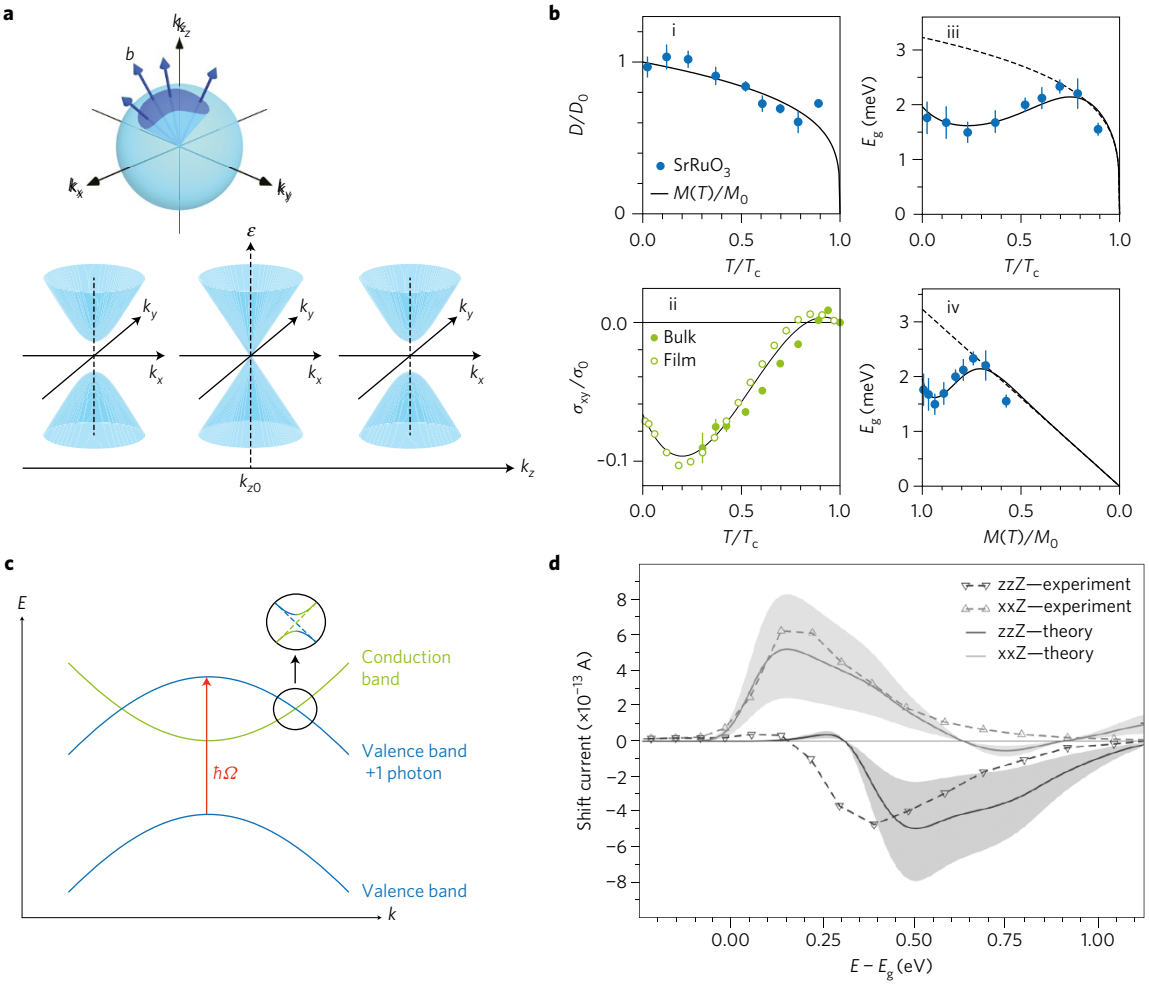

Figure 5 | Emergent electromagnetic field in momentum space. a, The band crossing in a ferromagnetic metal generating a magnetic monopole in momentum space. Upper panel: the distribution of the emergent magnetic field around a band crossing. Lower panel: the energy dispersion in the k_x–k_y plane for each k_z. The band crossing occurs at $k_z = k_{z0}$, which is described by a Weyl Hamiltonian. **b**, Magnon dynamics in an itinerant ferromagnet $SrRuO_3$. The energy dispersion is fitted well by the expression $\omega_q = E_g + Dq^2$, with q being the wavevector. The temperature dependence of D (i), E_g (iii), and anomalous Hall conductivity of both bulk and thin film samples (ii) are shown. Panel iv shows the fitting by a formula relating the anomalous Hall conductivity and the spin wave gap E_g assuming a Weyl fermion near the Fermi energy. The solid line in panel i is $M(T)/M$ (where $M(T)$ is the spontaneous magnetization at temperature T and $M = M(0)$), and the dashed lines in panels iii and iv are constant times $M(T)/M$. **c**, The schematic for the Floquet band, where the valence band is shifted by the energy of incident light $\hbar\Omega$. The anti-band crossings of the Floquet band is zoomed up[140]. **d**, Experiment and first-principles calculation of the shift current in $BiTiO_3$, which comes from the difference of the Berry connection between the conduction and valence bands. Reproduced from ref. 69, Macmillan Publishers Ltd (**a**); ref. 139, AAAS (**c**); and ref. 87, APS (**d**). Adapted from ref. 69, Macmillan Publishers Ltd (**b**).

field[102–107]. Experimental observations of this QAHE have been reported for thin films of the topological insulator $(Bi,Sb)_2Te_3$ doped with magnetic ions such as Cr and V (refs 105–107). The QAHE offers promising opportunities for spintronic functionalities, particularly the tunable domain boundaries. When a ferromagnetic topological insulator is in a single-domain state, spin-polarized helical current flows at the edge without energy dissipation. When antiparallel magnetic domains are arranged laterally, however, as shown in Fig. 6b, two helical currents with a potential of $U = \mu$ (red) and 0 (blue) merge at the boundary, resulting in an averaged $U = \mu/2$ (purple) without the loss of energy. Although energy dissipation occurs at the corner, where the purple arrows sink in the electrodes, as is the case for conventional QHE, this potential of dissipationless electron flow on reconfigurable domain walls/boundaries could be used as a state variable for information processing/storage devices. The domain wall is expected to be charged[108], and could be manipulated by electric field.

The Curie temperature of magnetically doped topological insulators varies with doping and is limited to 190 K (ref. 109), while the mass gap is estimated as large as about 50 meV (ref. 110). However, the QAHE has currently been realized only at very low temperature (<100 mK) for homogeneously doped thin films. The reason could be an inhomogeneity in the mass gap, composition or electrostatic potential, but this situation can be improved by magnetic modulation doping, as schematically shown in Fig. 6c. Concentrated magnetic elements are doped only in layers beneath the surfaces. As a matter of fact, the QAHE appears at a temperature as high as 2 K. To further enhance the stability of the QAHE, precise control of the Dirac point is required, along with high-quality heterostructures of pristine topological insulator and high-Curie-temperature ferromagnets[111].

Experiments on QAHE systems are still in their infancy, but interesting physical properties are starting to emerge, such as a quantized magneto-optical response in the terahertz regime (photon energy less than the mass gap)[112,113]. Faraday and Kerr rotations (θ_F, θ_K) of a terahertz pulse shone onto the QAHE state have been measured at 1.5 K and, taking into account the substrate[114] and multiple reflections, in the quantized limit, the

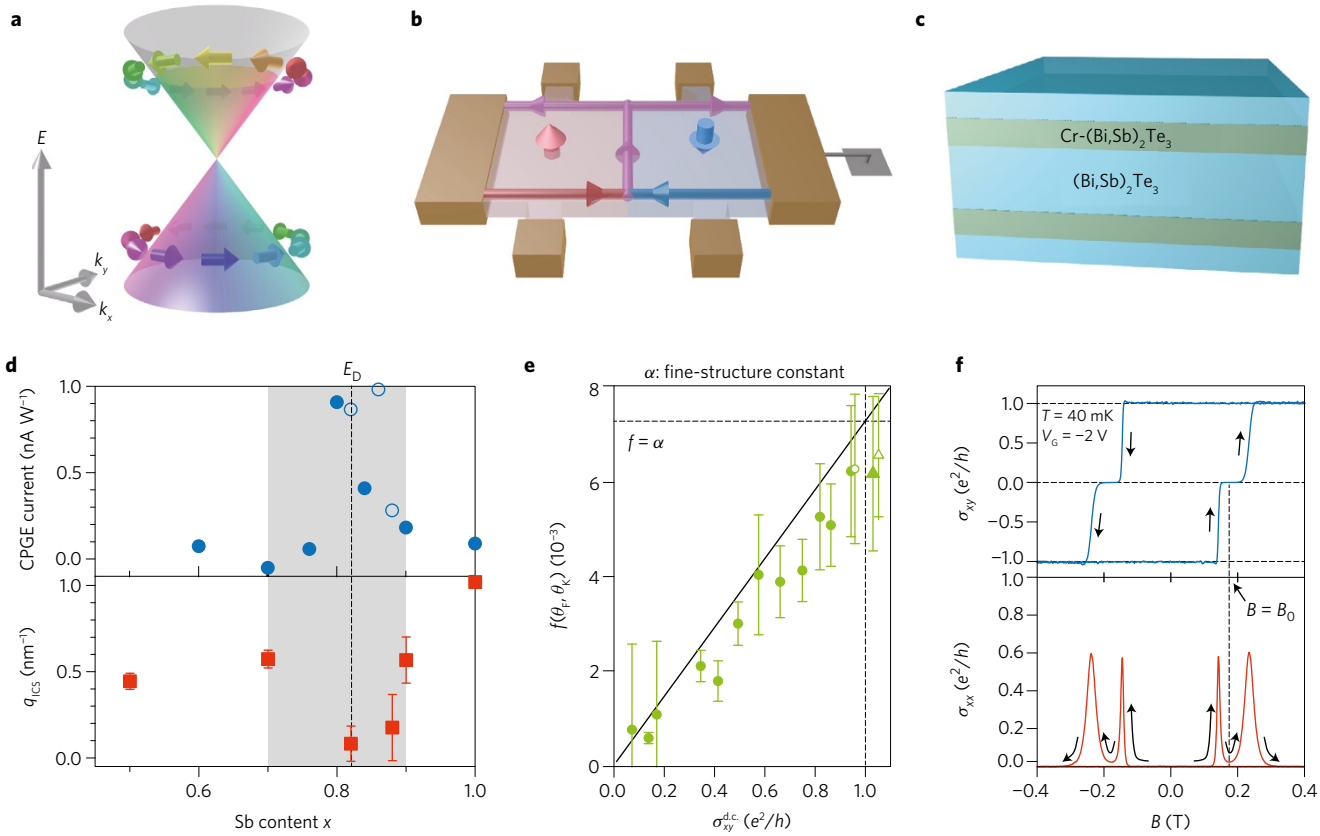

Figure 6 | Quantum phenomena observed in topological insulator heterostructures. a, Electronic structure of a surface state of a topological insulator in momentum space. **b**, Schematic of spin-polarized edge current in a ferromagnetic topological insulator in the quantum anomalous Hall state. Control of the magnetic domain structure results in the engineering of topological current flow. **c**, Magnetic modulation doping that yields clean surface states with enough magnetic coupling. **d**, Spontaneous photocurrent (circular photogalvanic effect current) in a topological insulator (top) and charge–spin conversion efficiency at a permalloy/topological insulator interface (bottom) as a function of chemical potential that is controlled by the Sb content in $(Bi_{1-x}Sb_x)_2Te_3$. E_D on the upper abscissa indicates E_F at the Weyl point and the hatched region denotes the region when E_F is within the bulk gap. **e**, Quantized magneto-optical rotation of terahertz light in the quantum anomalous Hall state. Evolution of the scaling function $f(\theta_F, \theta_K) = (\cot\theta_F - \cot\theta_K)/(\cot^2\theta_F - 2\cot\theta_F\cot\theta_K - 1)$ without any material parameters as a function of d.c. Hall conductance, which is expected to reach the fine structure constant α (~1/137) in the quantized limit, as indicated by a straight line. **f**, Transport properties in an asymmetric topological insulator heterostructure shown in **c**. Zero-Hall plateau with zero conductivity—that is, axion insulator state—is observed in an antiferromagnetic coupling state of the top and bottom surfaces. Adapted from ref. 98, APS (**d**, top); and ref. 101, Macmillan Publishers Ltd (**d**, bottom). Reproduced from ref. 115, Macmillan Publishers Ltd (**e**); and ref. 116, Macmillan Publishers Ltd (**f**).

function $f(\theta_F, \theta_K)$ should fall into the fine structure constant $\alpha = 2\pi e^2/hc \sim 1/137$. As shown in Fig. 6e, as the temperature is reduced σ_{xy} grows to e^2/h, and $f(\theta_F, \theta_K)$ increases linearly to reach α (ref. 115). When normalized by the thickness, the Faraday rotation for the QAHE film would be two orders of magnitude larger than those for representative magneto-optical materials, such as iron garnet.

By magnetic modulation doping, one can prepare a system known as an axion insulator, which shows a quantized magnetoelectric effect[116]. With different cohesive fields between up and down magnetic layers in Fig. 6c, an antiparallel magnetization can be realized. The magnetotransport properties, shown in Fig. 6f, clearly indicate a zero-Hall plateau $\sigma_{xy} = 0$ with $\sigma_{xx} = 0$ in antiparallel cases during magnetization reversal and $\sigma_{xy} = \pm e^2/h$ and $\sigma_{xx} = 0$ in parallel cases (QAHE) under saturation. This also enables magnetic-field-induced or gating-induced switching of the two-terminal resistance between h/e^2 (~26 kΩ in the QAHE state) and gigaohm range (for an axion insulator), realizing colossal magnetoresistance or electroresistance.

Turning to real space topology, the emergent electromagnetic fields e_α, b_α associated with skyrmions can produce novel and useful phenomena and functions, as shown schematically in Fig. 7a[57]. As skyrmions obtain gyrodynamics due to their nonzero skyrmion number N_{sk}, this means that a very small critical current density $j_c \sim 10^6$ A m^{-2} is needed to drive skyrmions compared with that of domain walls $j_c \sim 10^{11}$–10^{12} A m^{-2} (ref. 57). Various applications of skyrmions, such as magnetic memories, have been proposed and are being pursued towards 'skyrmionics'. Figure 7b shows an example where a racing circuit memory device, including the writing (creation), transfer (current-driven motion), reading (for example by magnetic tunnel junction), and deleting (annihilation) of skyrmions, is designed[117]. In three dimensions, the end point of a skyrmion string or the branching point of a skyrmion string into two is defined as a monopole[118,119], as schematically shown in Fig. 7c. As discussed in the section on Berry phase engineering, this monopole includes a singular magnetic configuration, at which the emergent magnetic field is also enhanced in a singular way, which could act as a promising source of strong emergent fields in real space.

Applications of emergent electromagnetism are a future issue. One possible application is an inductor that creates a voltage due to the change in the current via emergent electromagnetic induction. This possibility can be pursued both in the real and momentum spaces with the input of factors such as time-dependent currents,

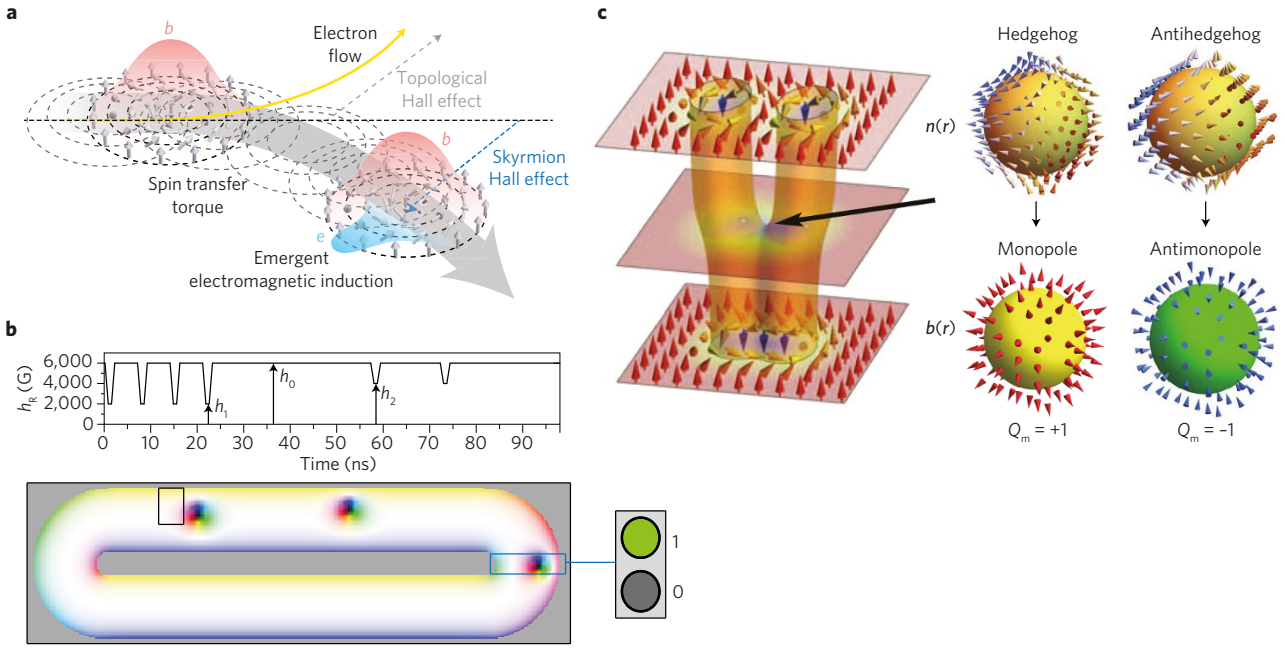

Figure 7 | Emergent electromagnetism in real space. a, The emergent electromagnetic phenomena related to a skyrmion. The emergent magnetic field b is accompanied by a skyrmion, which results in the topological Hall effect (THE) of the conduction electrons. On the other hand, the conduction current drives the motion of a skyrmion through the spin transfer torque effect, the trajectory of which is tilted slightly by the skyrmion Hall effect. Furthermore, the moving skyrmion and its emergent magnetic field result in the emergent electric field (electromagnetic induction). **b**, An example of the theoretical design of devices using skyrmions. The figure shows the racetrack memory of skyrmions, where the writing, transfer, readout, and erasing of skyrmions are numerically simulated. **c**, Monopole structure in real space. Left: monopole appearing at the branching point of a skyrmion string into two. Right: spin textures around the monopole and antimonopole and associated emergent magnetic field. Reproduced from ref. 57, Macmillan Publishers Ltd (**a**); ref. 118, AAAS (**c**, left); and ref. 119, Macmillan Publishers Ltd (**c**, right). Adapted from ref. 117, IOP (**b**).

electric fields, distortion, and pressure, which can produce emergent electric fields. This is connected to the idea of topological charge pumping, proposed by Thouless in the adiabatic limit[120].

Quantum computing

All modern computers are based on the binary system, with 0's and 1's, which fits perfectly to logical operations via Boolean algebra. And the 0 and 1 can be recorded as two states, such as on and off of a current or charge accumulation. This unit of information is called a 'bit'. Quantum computers, on the other hand, utilize the 'qubit', which is expressed by a linear combination of the two quantum states $|0\rangle$ and $|1\rangle$ as

$$|\psi\rangle = c_0|0\rangle + c_1|1\rangle \tag{2}$$

with c_0 and c_1 being complex numbers. It can be seen that a qubit contains much more information than the classical bit, and can be used for calculations that can never be achieved by classical computers, such as the factorization of large numbers. For that purpose, it is essential to keep the quantum coherency of the states. This is very difficult in solids, however, due to decoherence effects from the environments surrounding the qubit, but various possibilities are being pursued to overcome this problem, such as using the spin in a quantum dot[121] and superconducting qubits[122].

One promising way to resolve this issue is with topological quantum computing[123], exploiting Majorana fermions, which have several unique and useful features. The simplest model of the Majorana fermion has been proposed by Kitaev[124]. This is the model for a one-dimensional spinless p-wave superconductor, described by the Hamiltonian

$$H = -t\sum_{i=1}^{N-1}(c_i^+ c_{i+1} + \text{h.c.}) + \Delta\sum_{i=1}^{N-1}(c_i^+ c_{i+1}^+ + \text{h.c.}) \tag{3}$$

One can introduce the Majorana representation by expressing the complex creation and annihilation operators of electrons c_i^+ and c_i by Majorana operators (real fermion) a_i and b_i as

$$c_i^+ = \frac{1}{2}(a_i + ib_i), \quad c_i = \frac{1}{2}(a_i - ib_i) \tag{4}$$

where $a_i^+ = a_i$, $b_i^+ = b_i$ and $a_i^2 = b_i^2 = 1$ are satisfied. This representation decomposes the original electron into two Majorana fermions. The electron fractionalization is realized by the p-wave pairing represented by the order parameter Δ in equation (3). Especially when $t = \Delta$, equation (3) is reduced to

$$H = -it\sum_{i=1}^{N-1} a_i b_{i+1} \tag{5}$$

which means the 'dimerization' pattern of Majorana fermions. This dimerization leaves one Majorana fermion (b_1 at the left end and a_N at the right end) at each end of the system. This means that the electron is split between two Majorana fermions, separated by a gapped bulk state, constituting a doubly degenerate ground state. This non-local nature of Majorana fermions gives stability to the qubit, which makes Majorana fermions a promising candidate for a quantum information carrier. Physical realizations of the Kitaev model, and also of Majorana zero-energy bound states, have been pursued experimentally using quantum wires with spin–orbit interactions under magnetic fields, attached to the s-wave superconductor[125], and also with one-dimensional arrays of magnetic impurities on s-wave superconductors[126]. To truly establish a Majorana bound state, a smoking gun experiment, using a phase-sensitive probe, is still highly desirable[127,128]. Majorana fermions have special quantum statistics, known as non-Abelian statistics, that are described by a braid group, as shown in Fig. 8a[129–131]. Figure 8b shows one

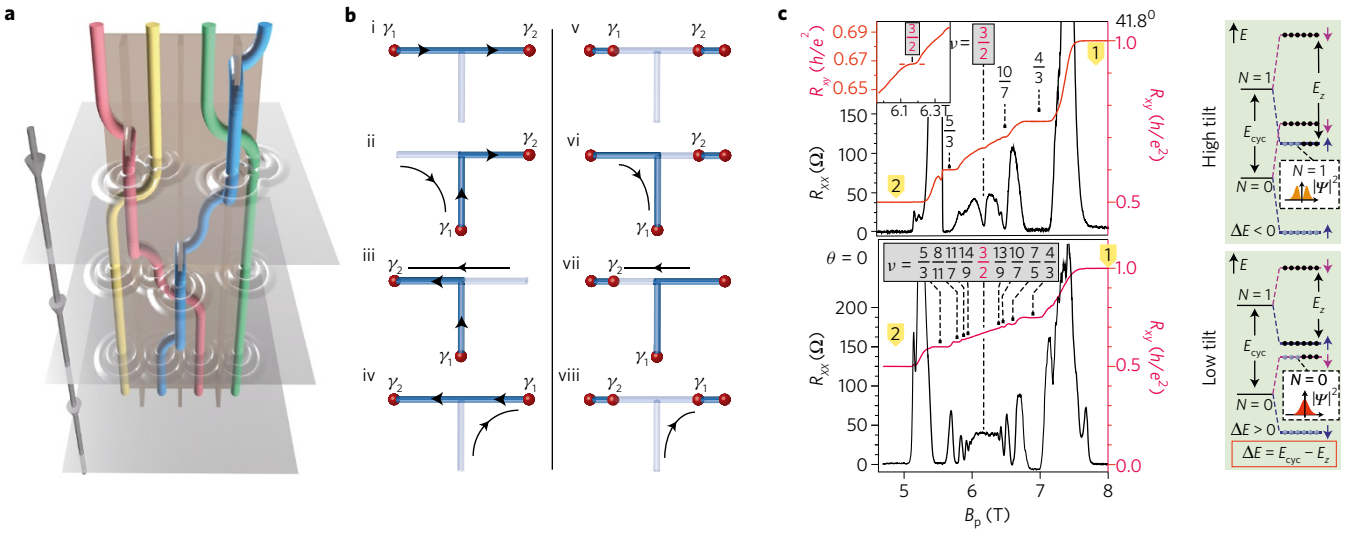

Figure 8 | Majorana fermions in topological superconductors and fractional quantum Hall systems. a, Braiding of four Majorana fermions showing the non-Abelian quantum statistics. **b**, The design of braiding Majorana fermions using the T-shaped one-dimensional system. **c**, Fractional QHE observed for a MgZnO/ZnO heterostructure under a tilted (top) and a perpendicular (bottom) magnetic field. The schematics on the right show spin-resolved energy levels. Although the filling is maintained at $\nu = 3/2$, the occupation of electrons shifts to the lower spin branch of the second Landau level as a result of the enhanced Zeeman energy in the high-tilt configuration. Reproduced from ref. 132, Macillan Publishers Ltd (**b**). Adapted from ref. 138, Macmillan Publishers Ltd (**c**).

way to realize a braiding operation in a T-shaped one-dimensional system[132]. This zero-energy Majorana bound state is also expected at the vortex core of a $p + ip$ chiral topological superconductor[130]. A similar situation can be realized when a two-dimensional superconductor is attached to the surface state of the three-dimensional topological insulator[133].

Another possible candidate to realize Majorana fermions is in two-dimensional semiconductors showing the fractional quantum Hall effect (FQHE) or, more specifically, those which belong to a Moore–Read Pfaffian state[134]. The QHE takes place not only at integer fillings but also at fractional values as a result of electron correlation effects[135]. One successful model of the FQHE is based on 'composite fermions', where the interaction energy is minimized by forming composite particles of electrons attached to a discrete number of magnetic flux quanta[136]. A vast array of states has now been observed where, in general, ν takes an odd denominator as a result of the Pauli exclusion principle. The most remarkable exception to this has been the FQHE at $\nu = 5/2$ in GaAs heterostructures[137]. Its most widely accepted explanation is that an attractive interaction occurs between composite fermions within the second Landau level, owing to the nodal nature of the electronic wavefunction. This leads to a type of 'chiral superconducting state' with the pairing of the two composite fermions. Its wavefunction may be described by the Moore–Read Pfaffian state, with the corresponding quasi-particles expected to obey non-Abelian statistics.

Recently, such an even denominator state was discovered in MgZnO/ZnO heterostructures at $\nu = 3/2$ (ref. 138). In the ZnO system, the cyclotron (E_{cyc}) and Zeeman (E_z) splitting of Landau levels becomes comparable, allowing experimental control over the crossing of spin-resolved Landau levels by tilting the magnetic field. At $\theta = 0°$, conventional odd denominator FQHE is observed, consistent with composite fermions from the lowest Landau level, while at $\theta \sim 42°$ the $\nu = 3/2$ state emerges, as shown in Fig. 8c. The energy level constellation of this transition is shown in the right-hand panels, where spin-resolved Landau levels are schematically shown for the high-tilt and low-tilt configurations. This leads to the model in which the $\nu = 3/2$ state is an analogue of the $\nu = 5/2$ state that occurs in the GaAs system. This result demonstrates that even denominator states are a universal phenomenon and the filling of spin-resolved Landau levels is unique to their stabilization. More distinctive for ZnO is the tunability of the state through Zeeman-splitting-induced level crossing; this opens a new experimental avenue to verify the applicability of the Pfaffian state description, along with its true nature, that otherwise may not be possible.

Outlook

On the basis of the concept illustrated in Fig. 1b, we have described how and why quantum materials can be the platform of emergent functions. Among them, the contemporary and future societal demands for better electronics for information processing, as exemplified by (1) ultralow energy consumption, (2) high speed, (3) huge capacity, and (4) high security. Quantum materials can contribute to these requirements in a ground-breaking manner: Mottronics for (1)–(3); magnetoelectrics for (1); topological electronics for (1)–(3); and quantum computing for (2)–(4); as outlined in this article.

The conceptual basis throughout quantum-materials-based electronics is strong correlation and topology. Electron correlation occasionally defines classical order parameters, which can be used as state variables for their operation. Those include not only ferromagnetic and ferroelectric orders, but also potentially many other magnetic, orbital, charge, and their combined (multiferroic) orders, irrespective of their commensurate or incommensurate form, as long as they can be clearly defined as writable, controllable and readable variables for the operation.

Next-generation electronics will be able to make use of the expanded concept of 'current' as the non-local transmission of state variables. Among them, topological currents in quantum materials are the most important notion, as exemplified by the edge currents of the quantum Hall state, but there are other examples, such as spin and polarization currents. Topological currents, when coupled to the order parameter, can also be a source of abundant nonlinear and nonreciprocal response functions. These nonreciprocal responses may play the role of one-way transmission of the generalized currents, and hence of information.

Another important aspect of quantum materials is topological protection, which assures stability of a quantum state. The robustness of topologically protected states against external disturbances is a prerequisite for the operation of state variables,

Table 1 | Summary of various emergent functions discussed in this article.

Emergent functions	Key concept	Control parameter	Bottleneck/key experiment	Target industry
Mottronics	Electron correlation	Band-filling Bandwidth	E-field switching at RT Above-RT superconductor	Low-energy-cost electronics Energy harvesting/saving
Magnetoelectrics	Spin–orbit interaction	Broken symmetries both in space and time	E-field switching at RT Ultrafast photo-switching	Low-energy-cost electronics Information technology
Topological electronics	Berry phase	Band structure design Spin texture	Zero-field edge current at RT Skyrmionic circuit	Information technology Energy harvesting
Quantum computing	Quantum coherence	Nanomaterials design Topological protection	Qubit/photon interface Quantum simulator	Quantum computer Information security

as exemplified by Majorana fermions, which have applications in topological quantum computation. Highly robust metastable skyrmions and dissipationless edge current in quantum Hall or quantum anomalous Hall states are other examples of topologically protected states.

Energy-harvesting functions are also highly desirable, equivalent to the conversion of energy forms from light to electricity (photovoltaics or solar cells), from chemical energy to electricity (batteries), and from thermal energy to electricity (thermoelectrics). From the viewpoint of energy conversion, strongly correlated systems offer a good laboratory since many different inputs and outputs—different forms of energy—are coupled simultaneously through the entangled internal degrees of freedom, as shown in Fig. 1b. The topological nature of some quantum materials could also be relevant to energy harvesting. For example, dissipationless shift currents (mentioned above) could be related to a photovoltaic-like action. This is also an example of a nonlinear phenomena of many-body electrons in non-equilibrium states. These are difficult problems both experimentally and theoretically, but they are a fertile field waiting for challenges.

To summarize the discussion in this review, the key concept, control parameters, bottleneck/key experiments, and target industry for each of the emergent functions are listed in Table 1. On the basis of emergence in many-body systems, quantum materials offer the most promising means to bridge three major issues in science: energy, matter, and information.

Received 6 March 2017; accepted 25 August 2017; published online 25 September 2017; corrected online 17 October 2017

References

1. Anderson, P. W. More is different. *Science* **177,** 393–396 (1972).
2. King-Smith, R. D. & Vanderbilt, D. Theory of polarization of crystalline solids. *Phys. Rev. B* **47,** R1651–R1654 (1993).
3. Resta, R. Macroscopic electric polarization as a geometric quantum phase. *Europhys. Lett.* **22,** 133–138 (1993).
4. Berry, M. V. Quantal phase factors accompanying adiabatic changes. *Proc. R. Soc. Lond. A* **392,** 45–57 (1984).
   The original paper of Berry phase revealing the geometrical nature of quantum mechanics.
5. Tokura, Y. Correlated-electron physics in transition-metal oxides. *Phys. Today* **56,** 50–55 (July, 2003).
6. Imada, M., Fujimori, A. & Tokura, Y. Metal–insulator transitions. *Rev. Mod. Phys.* **70,** 1039–1263 (1998).
   A review on the physics of strong electron correlation and Mott transition including many experimental results.
7. Lee, P. A., Nagaosa, N. & Wen, X.-G. Doping a Mott insulator: physics of high-temperature superconductivity. *Rev. Mod. Phys.* **78,** 17–85 (2006).
   A review on theories and experiments on cuprates superconductors from the viewpoint of strong electron correlation.
8. Gao, L. *et al*. Superconductivity up to 164 K in $HgBa_2Ca_{m-1}Cu_mO_{2m+2+\delta}$ ($m=1$, 2, and 3) under quasihydrostatic pressures. *Phys. Rev. B* **50,** 4260–4263 (1994).
9. Yamamoto, A., Takeshita, N., Terakura, C. & Tokura, Y. High pressure effects revisited for the cuprate superconductor family with highest critical temperature. *Nat. Commun.* **6,** 8990 (2015).
10. Drozdov, A. P., Eremets, M. I., Trojan, I. A., Ksenofontov, V. & Shylin, S. I. Conventional superconductivity at 203 kelvin at high pressures in the sulfur hydride system. *Nature* **525,** 73–76 (2015).
    The report on the experimental discovery of superconductivity in sulfur hydride under high pressure with the highest transition temperature at present.
11. Shinohara, Y., Taneda, T. & Yoshizumi, M. Overview of materials and power applications of coated conductors project. *Jpn. J. Appl. Phys.* **51,** 010007 (2012).
12. Sato, K., Kobayashi, S. & Nakashima, T. Present status and future perspective of bismuth-based high-temperature superconducting wires realizing application systems. *Jpn. J. Appl. Phys.* **51,** 010006 (2012).
13. Krause, H.-J. & Kreutzbruck, M. V. Recent developments in SQUID NDE. *Physica C* **368,** 70–79 (2002).
14. Tokura, Y. & Nagaosa, N. Orbital physics in transition-metal oxides. *Science* **288,** 462–468 (2000).
15. Tokura, Y. Critical features of colossal magnetoresistive manganites. *Rep. Prog. Phys.* **69,** 797–851 (2006).
    The review article on colossal magnetoresistance in manganites providing the explanation of its physical mechanisms.
16. Kuwahara, H. *et al*. Striction-coupled magnetoresistance in perovskite-type manganese oxides. *Science* **272,** 80–82 (1996).
17. Fiebig, M., Miyano, K., Tomioka, T. & Tokura, Y. Visualization of the local insulator–metal transition in $Pr_{0.7}Ca_{0.3}MnO_3$. *Science* **280,** 1925–1928 (1998).
18. Nakano, M. *et al*. Collective bulk carrier delocalization driven by electrostatic surface charge accumulation. *Nature* **487,** 459–462 (2012).
19. Jeong, J. *et al*. Suppression of metal–insulator transition in VO_2 by electric field-induced oxygen vacancy formation. *Science* **339,** 1402–1405 (2013).
20. Nakano, M. *et al*. Infrared-sensitive electrochromic device based on VO_2. *Appl. Phys. Lett.* **103,** 153503 (2013).
21. Waser, R. & Aono, M. Nanoionics-based resistive switching memories. *Nat. Mater.* **6,** 833–840 (2007).
22. Sawa, A. Resistive switching in transition metal oxides. *Mater. Today* **11,** 28–36 (June 2008).
23. Sawa, A., Fujii, T., Kawasaki, M. & Tokura, Y. Hysteretic current-voltage characteristics and resistance switching at a rectifying $Ti/Pr_{0.7}Ca_{0.3}MnO_3$ interface. *Appl. Phys. Lett.* **85,** 4073–4075 (2004).
24. Liu, S. Q., Wu, N. J. & Ignatiev, A. Electric-pulse-induced reversible resistance change effect in magnetoresistive films. *Appl. Phys. Lett.* **76,** 2749–2751 (2000).
25. Tokura, Y. Photoinduced phase transition: A tool for generating a hidden state of matter. *J. Phys. Soc. Jpn* **75,** 011001 (2006).
26. Hu, W. *et al*. Optically enhanced coherent transport in $YBa_2Cu_3O_{6.5}$ by ultrafast redistribution of interlayer coupling. *Nat. Mater.* **13,** 705–711 (2014).
27. Mitrano, M. *et al*. Possible light-induced superconductivity in K_3C_{60} at high temperature. *Nature* **530,** 461–464 (2016).
28. Dzyaloshinskii, I. E. On the magneto-electrical effect in antiferromagnets. *Sov. Phys. JETP* **10,** 628–629 (1959).
29. Astrov, D. N. The magnetoelectric effect in antiferromagnets. *Sov. Phys. JETP* **11,** 708–709 (1960).
30. Remeika, J. P. $GaFeO_3$; a ferromagneteic-piezoelectric compound. *J. Appl. Phys.* **31,** 263S–264S (1960).
31. Arima, T. *et al*. Structural and magnetoelectric properties of $Ga_{2-x}Fe_xO_3$ single crystals grown by a floating-zone method. *Phys. Rev. B* **70,** 064426 (2004).

32. Kurumaji, T., Ishiwata, S. & Tokura, Y. Doping-tunable ferrimagnetic phase with large linear magnetoelectric effect in a polar magnet $Fe_2Mo_3O_8$. *Phys. Rev. X* **5,** 031034 (2015).
33. Spaldin, N. A., Cheong, S.-W. & Ramesh, R. Multferroics: past, present, and future. *Phys. Today* **63,** 38–43 (October, 2010).
34. Tokura, Y. Multiferroics as quantum electromagnets. *Science* **312,** 1481–1482 (2006).
35. Khomskii, D. Classifying multiferroics: mechanisms and effects. *Physics* **2,** 20 (2009).
36. Ramesh, R. & Spaldin, N. A. Multiferroics: progress and prospects in thin films. *Nat. Mater.* **6,** 21–29 (2007).
37. Catalan, G. & Scott, J. F. Physics and applications of bismuth ferrite. *Adv. Mater.* **21,** 2463–2485 (2009).
38. Fiebig, M. Revival of the magnetoelectric effect. *J. Phys. D: Appl. Phys.* **38,** R123–R152 (2005).
39. Tokura, Y., Seki, S. & Nagaosa, N. Multiferroics of spin origin. *Rep. Prog. Phys.* **77,** 076501 (2014).
A review on multiferroics of spin origin systematically classifying the mechanisms for variety of materials.
40. Arima, T. Ferroelectricity induced by proper-screw type magnetic order. *J. Phys. Soc. Jpn* **76,** 073702 (2007).
41. Tokunaga, Y. *et al*. Composite domain walls in a multiferroic perovskite ferrite. *Nat. Mater.* **8,** 558–562 (2009).
42. Tokunaga, Y., Taguchi, Y., Arima, T. & Tokura, Y. Electric-field-induced generation and reversal of ferromagnetic moment in ferrites. *Nat. Phys.* **8,** 838–844 (2012).
43. Soda, M., Ishikura, T., Nakamura, H., Wakabayashi, Y. & Kimura, T. Magnetic ordering in relation to the room-temperature magnetoelectric effect of $Sr_3Co_2Fe_{24}O_{41}$. *Phys. Rev. Lett.* **106,** 087201 (2011).
44. Chun, S.-H. *et al*. Electric field control of nonvolatile four-state magnetization at room temperature. *Phys. Rev. Lett.* **108,** 177201 (2012).
45. Matsukura, F., Tokura, Y. & Ohno, H. Control of magnetism by electric fields. *Nat. Nanotech.* **10,** 209–220 (2015).
46. Takahashi, Y., Yamasaki, Y. & Tokura, Y. Terahertz magnetoelectric resonance enhanced by mutual coupling of electromagnons. *Phys. Rev. Lett.* **111,** 037204 (2013).
47. Katsura, H., Balatsky, A. V. & Nagaosa, N. Dynamical magnetoelectric coupling in helical magnets. *Phys. Rev. Lett.* **98,** 027203 (2007).
48. Pimenov, A. *et al*. Possible evidence for electromagnons in multiferroic manganites. *Nat. Phys.* **2,** 97–100 (2006).
49. Kimura, T., Lawes, G. & Ramirez, A. P. Electric polarization rotation in a hexaferrite with long-wavelength magnetic structures. *Phys. Rev. Lett.* **94,** 132701 (2005).
50. Ishiwata, S., Taguchi, Y., Murakawa, H., Onose, Y. & Tokura, Y. Low-magnetic-field control of electric polarization vector in a helimagnet. *Science* **319,** 1643–1646 (2008).
51. Kézsmárki, I. *et al*. Enhanced directional dichroism of terahertz light in resonance with magnetic excitations of the multiferroic $Ba_2CoGe_2O_7$ oxide compound. *Phys. Rev. Lett.* **106,** 057403 (2011).
52. Saito, M., Taniguchi, K. & Arima, T. Gigantic optical magnetoelectric effect in CuB_2O_4. *J. Phys. Soc. Jpn* **77,** 013705 (2008).
53. Xiao, D., Chang, M.-C. & Niu, Q. Berry phase effects on electronic properties. *Rev. Mod. Phys.* **82,** 1959–2007 (2010).
A review article on Berry phase based on the semiclassical wavepacket formalism that includes many applications, most of which are to condensed matter physics.
54. Nagaosa, N., Sinova, J., Onoda, S., MacDonald, A. H. & Ong, N. P. Anomalous Hall effect. *Rev. Mod. Phys.* **82,** 1539–1592 (2010).
55. Taguchi, Y., Oohara, Y., Yoshizawa, H., Nagaosa, N. & Tokura, Y. Spin chirality, Berry phase and anomalous Hall effect in a frustrated ferromagnet. *Science* **291,** 2573–2576 (2001).
56. Taguchi, Y. *et al*. Magnetic field induced sign reversal of the anomalous Hall effect in a pyrochlore ferromagnet $Nd_2Mo_2O_7$: evidence for a spin chirality mechanism. *Phys. Rev. Lett.* **90,** 257202 (2003).
57. Nagaosa, N. & Tokura, Y. Topological properties and dynamics of magnetic skyrmions. *Nat. Nanotech.* **8,** 899–911 (2013).
A review article on the skyrmions and their dynamics in magnets from the viewpoint of topology and emergent electromagnetism due to Berry phase.
58. Oike, H. *et al*. Interplay between topological and thermodynamic stability in a metastable magnetic skyrmion lattice. *Nat. Phys.* **12,** 62–66 (2016).
59. Schulz, T. *et al*. Emergent electrodynamics of skyrmions in a chiral magnet. *Nat. Phys.* **8,** 301–304 (2012).
An experiment to observe the emergent electromagnetic induction in terms of the Hall effect in skyrmion system.
60. Kanazawa, N. *et al*. Large topological Hall effect in a short-period helimagnet MnGe. *Phys. Rev. Lett.* **106,** 156603 (2011).
61. Nagaosa, N., Yu, X. Z. & Tokura, Y. Gauge fields in real and momentum spaces in magnets: monopoles and skyrmions. *Phil. Trans. R. Soc. A* **370,** 5806–5819 (2012).
62. Milde, P. *et al*. Unwinding of a skyrmion lattice by magnetic monopoles. *Science* **340,** 1076–1080 (2013).
63. Adams, E. N. & Blount, E. I. Energy bands in the presence of an external force field–II. Anomalous velocities. *J. Phys. Chem. Solids* **10,** 286–303 (1959).
64. Prange, R. E. & Girvin, S. M. *The Quantum Hall Effect* (Springer, 1987).
A comprehensive textbook on the quantum Hall effect summarizing the knowledge up to that time.
65. von Klitzing, K., Dorda, G. & Pepper, M. New method for high-accuracy determination of the fine-structure constant based on quantized Hall resistance. *Phys. Rev. Lett.* **45,** 494–497 (1980).
The original experimental paper of integer quantum Hall effect, which opened up the researches on topological properties of electrons in solids.
66. Murakami, S. & Nagaosa, N. Spin Hall effect. *Comprehensive Semiconductor Science and Technology* Vol. 1, 222–278 (Elsevier, 2011).
67. Thouless, D. J., Kohmoto, M., Nightingale, M. P. & den Nijs, M. Quantized Hall conductance in a two-dimensional periodic potential. *Phys. Rev. Lett.* **49,** 405–408 (1982).
The original theory paper connecting the topological number to the Hall conductance so-called TKNN formula.
68. Fang, Z. *et al*. The anomalous Hall effect and magnetic monopoles in momentum space. *Science* **302,** 92–95 (2003).
69. Itoh, S. *et al*. Weyl fermions and spin dynamics of metallic $SrRuO_3$. *Nat. Commun.* **7,** 11788 (2016).
70. Vafek, O. & Vishwanath, A. Dirac fermions in solids: from high-T_c cuprates and graphene to topological insulators and Weyl semimetals. *Annu. Rev. Condens. Matter Phys.* **5,** 83–112 (2014).
71. Castro Neto, A. H., Guinea, F., Peres, N. M. R., Novoselov, K. S. & Geim, A. K. The electronic properties of graphene. *Rev. Mod. Phys.* **81,** 109–162 (2009).
72. Nielsen, H. B. & Ninomiya, M. A no-go theorem for regularizing chiral fermions. *Phys. Lett.* **B105,** 219–223 (1981).
73. Wan, X., Turner, A. M., Vishwanath, A. & Savrasov, S. Y. Topological semimetal and Fermi-arc surface states in the electronic structure of pyrochlore iridates. *Phys. Rev. B* **83,** 205101 (2011).
Prediction of the Weyl semimetal in pyrochlore iridates, which triggered the intensive researches on Weyl fermion.
74. Fujikawa, K. & Suzuki, H. *Path Integrals and Quantum Anomalies* (International Series of Monographs on Physics, Oxford Univ. Press, 2004).
75. Fukushima, K., Kharzeev, D. E. & Warringa, H. J. Chiral magnetic effect. *Phys. Rev. D* **78,** 074033 (2008).
76. Huang, X. *et al*. Observation of the chiral-anomaly-induced negative magnetoresistance in 3D Weyl semimetal TaAs. *Phys. Rev. X* **5,** 031023 (2015).
77. Onoda, M., Murakami, S. & Nagaosa, N. Hall effect of light. *Phys. Rev. Lett.* **93,** 083901 (2004).
78. Haldane, F. D. M. & Raghu, S. Possible realization of directional optical waveguides in photonic crystals with broken time-reversal symmetry. *Phys. Rev. Lett.* **100,** 013904 (2008).
79. Katsura, H., Nagaosa, N. & Lee, P. A. Theory of the thermal Hall effect in quantum magnets. *Phys. Rev. Lett.* **104,** 066403 (2010).
80. Onose, Y. *et al*. Observation of the magnon Hall effect. *Science* **329,** 297–299 (2010).
81. Matsumoto, R. & Murakami, S. Rotational motion of magnons and the thermal Hall effect. *Phys. Rev. B* **84,** 184406 (2011).
82. Grinberg, I. *et al*. Perovskite oxides for visible-light-absorbing ferroelectric and photovoltaic materials. *Nature* **503,** 509–512 (2013).
83. Nie, W. *et al*. High-efficiency solution-processed perovskite solar cells with millimeter-scale grains. *Science* **347,** 522–525 (2015).
84. Shi, D. *et al*. Low trap-state density and long carrier diffusion in organolead trihalide perovskite single crystals. *Science* **347,** 519–522 (2015).
85. de Quilettes, D. W. *et al*. Impact of microstructure on local carrier lifetime in perovskite solar cells. *Science* **348,** 683–686 (2015).
86. Bhatnagar, A., Chaudhuri, A. R., Kim, Y. H., Hesse, D. & Alexe, M. Role of domain walls in the abnormal photovoltaic effect in $BiFeO_3$. *Nat. Commun.* **4,** 2835 (2013).
87. Young, S. M. & Rappe, A. M. First principles calculation of the shift current photovoltaic effect in ferroelectrics. *Phys. Rev. Lett.* **109,** 116601 (2012).
88. Frost, J. M. *et al*. Atomistic origins of high-performance in hybrid halide perovskite solar cells. *Nano Lett.* **14,** 2584–2590 (2014).
89. Hwang, H. Y. *et al*. Emergent phenomena at oxide interfaces. *Nat. Mater.* **11,** 103–113 (2012).
90. Yao, W., Xiao, D. & Niu, Q. Valley-dependent optoelectronics from inversion symmetry breaking. *Phys. Rev. B* **77,** 235406 (2008).

91. Fisher, M. E. & Nagaosa, N. Profile of David J. Thouless, J. Michael Kosterlitz, and F. Duncan M. Haldane, 2016 Nobel Laureates in Physics. *Proc. Natl Acad. Sci. USA* **114,** 626–628 (2017).
92. Qi, X.-L. & Zhang, S.-C. The quantum spin Hall effect and topological insulators. *Phys. Today* **63,** 33–38 (January, 2010).
93. Hasan, M. Z. & Kane, C. L. Colloquium: topological insulators. *Rev. Mod. Phys.* **82,** 3045–3067 (2010).
A comprehensive review article on topological insulators for general readership.
94. Qi, X.-L. & Zhang, S.-C. Topological insulators and superconductors. *Rev. Mod. Phys.* **83,** 1057–1110 (2011).
95. Schnyder, A. P., Ryu, S., Furusaki, A. & Ludwig, A. W. W. Classification of topological insulators and superconductors in three spatial dimensions. *Phys. Rev. B* **78,** 195125 (2008).
96. Halperin, B. I. Quantized Hall conductance, current-carrying edge states, and the existence of extended states in a two-dimensional disordered potential. *Phys. Rev. B* **25,** 2185–2190 (1982).
97. Mclver, K. W., Hsieh, D., Steinberg, H., Jarillo-Herrero, P. & Gecik, N. Control over topological insulator photocurrents with light polarization. *Nat. Nanotech.* **7,** 96–100 (2012).
98. Okada, K. N. *et al*. Enhanced photogalvanic current in topological insulators via Fermi energy tuning. *Phys. Rev. B* **93,** 081403(R) (2016).
99. Bychkov, Y. A. & Rashba, E. I. Properties of a 2D electron gas with lifted spectral degeneracy. *JETP Lett.* **39,** 78–81 (1984).
100. Edelstein, V. M. Spin polarization of conduction electrons induced by electric current in two-dimensional asymmetric electron systems. *Solid State Commun.* **73,** 233–235 (1990).
101. Kondou, K. *et al*. Fermi-level-dependent charge-to-spin current conversion by Dirac surface states of topological insulators. *Nat. Phys.* **12,** 1027–1031 (2016).
102. Haldane, F. D. M. Model for a quantum Hall effect without Landau levels: condensed-matter realization of the "parity anomaly". *Phys. Rev. Lett.* **61,** 2015–2018 (1988).
103. Onoda, M. & Nagaosa, N. Quantized anomalous Hall effect in two-dimensional ferromagnets: quantum Hall effect in metals. *Phys. Rev. Lett.* **90,** 206601 (2003).
104. Yu, R. *et al*. Quantized anomalous Hall effect in magnetic topological insulators. *Science* **329,** 61–64 (2010).
105. Chang, C.-Z. *et al*. Experimental observation of the quantum anomalous Hall effect in a magnetic topological insulator. *Science* **340,** 167–170 (2013).
Experimental discovery of the quantized anomalous Hall effect in magnetic topological insulators under zero magnetic field.
106. Checkelsky, J. G. *et al*. Trajectory of the anomalous Hall effect towards the quantized state in a ferromagnetic topological insulator. *Nat. Phys.* **10,** 731–736 (2014).
107. Chang, C.-Z. *et al*. High-precision realization of robust quantum anomalous Hall state in a hard ferromagnetic topological insulator. *Nat. Mater.* **14,** 773–477 (2015).
108. Nomura, K. & Nagaosa, N. Electric charging of magnetic textures on the surface of a topological insulator. *Phys. Rev. B* **82,** 161401(R) (2010).
109. Zhou, Z., Chien, Y.-J. & Uher, C. Thin film dilute ferromagnetic semiconductors $Sb_{2-x}Cr_xTe_3$ with a Curie temperature up to 190 K. *Phys Rev. B* **74,** 224418 (2006).
110. Lee, I. *et al*. Imaging Dirac-mass disorder from magnetic dopant atoms in the ferromagnetic topological insulator $Cr_x(Bi_{0.1}Sb_{0.9})_{2-x}Te_3$. *Proc. Natl Acad. Sci. USA* **112,** 1316–1321 (2015).
111. Katmis, F. *et al*. A high-temperature ferromagnetic topological insulating phase by proximity coupling. *Nature* **533,** 513–516 (2016).
112. Qi, X.-L., Hughes, T. L. & Zhang, S.-C. Topological field theory of time-reversal invariant insulators. *Phys. Rev. B* **78,** 195424 (2008).
Field theoretical treatment of topological insulators and predictions of their physical properties.
113. Tse, W. K. & MacDonald, A. H. Giant magneto-optical Kerr effect and universal Faraday effect in thin-film topological insulators. *Phys. Rev. Lett.* **105,** 057401 (2010).
114. Maciejko, J., Qi, X.-L., Drew, H. D. & Zhang, S.-C. Topological quantization in units of the fine structure constant. *Phys. Rev. Lett.* **105,** 166803 (2010).
115. Okada, K. N. *et al*. Terahertz spectroscopy on Faraday and Kerr rotations in a quantum anomalous Hall state. *Nat. Commun.* **7,** 12245 (2016).
116. Mogi, M. *et al*. A magnetic heterostructure of topological insulators: a candidate for axion insulator. *Nat. Mater.* **16,** 516–521 (2017).
117. Koshibae, W. *et al*. Memory functions of magnetic skyrmions. *Jpn. J. Appl. Phys.* **54,** 053001 (2015).
118. Milde, P. *et al*. Unwinding of a skyrmion lattice by magnetic monopoles. *Science* **340,** 1076–1080 (2013).
119. Kanazawa, N. *et al*. Critical phenomena of emergent magnetic monopoles in a chiral magnet. *Nat. Commun.* **7,** 11622 (2016).
120. Thouless, D. J. Quantization of particle transport. *Phys. Rev. B* **27,** 6083–6087 (1983).
121. Loss, D. & DiVincenzo, D. P. Quantum computation with quantum dots. *Phys. Rev. A* **57,** 120–126 (1998).
122. Nakamura, Y., Pashkin, Y. A. & Tsai, J. S. Coherent control of macroscopic quantum states in a single-Cooper-pair box. *Nature* **398,** 786–788 (1999).
123. Sarma, S. D., Freedman, M. & Nayak, C. Topological quantum computation. *Phys. Today* **59,** 32–38 (July, 2006).
124. Kitaev, A. Unpaired Majorana fermions in quantum wires. *Proc. Mesoscopic Strongly Correlated Electron Systems Conference* (9–16 July 2000, Chernogolovka, Moscow Region, Russia); http://arXiv.org/abs/cond-mat/0010440
125. Mourik, V. *et al*. Signatures of Majorana fermions in hybrid superconductor-semiconductor nanowire devices. *Science* **336,** 1003–1007 (2012).
Early experimental report on the Majorana bound state at the ends of a semiconductor nanowire with spin–orbit interaction on a superconductor.
126. Nadj-Perge, S. *et al*. Observation of Majorana fermions in ferromagnetic atomic chains on a superconductor. *Science* **346,** 602–607 (2014).
127. Akhmerov, A. R., Nilsson, J. & Beenakker, C. W. J. Electrically detected interferometry of Majorana fermions in a topological insulator. *Phys. Rev. Lett.* **102,** 216404 (2009).
128. Law, K. T., Lee, P. A. & Ng, T. K. Majorana fermion induced resonant Andreev reflection. *Phys. Rev. Lett.* **103,** 237001 (2009).
129. Nayak, C., Simon, S. H., Stern, A., Freedman, M. & Sarma, S. D. Non-Abelian anyons and topological quantum computation. *Rev. Mod. Phys.* **80,** 1083–1159 (2008).
130. Ivanov, A. Non-Abelian statistics of half-quantum vortices in p-wave superconductors. *Phys. Rev. Lett.* **86,** 268–271 (2001).
131. Alicea, J. New directions in the pursuit of Majorana fermions in solid state systems. *Rep. Prog. Phys.* **75,** 076501 (2012).
132. Alicea, J., Oreg, Y., Refael, G., von Oppen, F. & Fisher, M. P. A. Non-Abelian statistics and topological quantum information processing in 1D wire networks. *Nat. Phys.* **7,** 412–417 (2011).
133. Fu, L. & Kane, C. L. Superconducting proximity effect and Majorana fermions at the surface of a topological insulator. *Phys. Rev. Lett.* **100,** 096407 (2008).
134. Moore, G. & Read, N. Nonabelions in the fractional quantum Hall effect. *Nucl. Phys. B* **360,** 362–396 (1991).
135. Tsui, D. C., Stormer, H. L. & Gossard, A. C. Two-dimensional magnetotransport in the extreme quantum limit. *Phys. Rev. Lett.* **48,** 1559–1562 (1982).
136. Jain, J. K. Composite-fermion approach for the fractional quantum Hall effect. *Phys. Rev. Lett.* **63,** 199–203 (1989).
137. Willett, R. *et al*. Observation of an even-denominator quantum number in the fractional quantum Hall effect. *Phys. Rev. Lett.* **59,** 1776–1779 (1987).
138. Falson, J. *et al*. Even-denominator fractional quantum Hall physics in ZnO. *Nat. Phys.* **11,** 347–351 (2015).
139. Morimoto, T. & Nagaosa, N. Topological nature of nonlinear optical effects in solids. *Sci. Adv.* **2,** e1501524 (2016).
140. Morimoto, T. & Nagaosa, N. Topological aspects of nonlinear excitonic processes in noncentrosymmetric crystals. *Phys. Rev. B* **94,** 035117 (2016).

Acknowledgements

The authors would like to thank M. Uchida, M. Ishida and C. Terakura for their help in preparing the manuscript.

Additional information

Competing financial interests

The authors declare no competing financial interests.

Erratum: Emergent functions of quantum materials

Yoshinori Tokura, Masashi Kawasaki and Naoto Nagaosa

Nature Physics http://doi.org/10.1038/nphys4274 (2017); published online 25 August 2017; corrected online 17 October 2017

In the version of this Review originally published, the notes accompanying refs 4, 6, 7, 10, 15, 39, 53, 57, 59, 64, 65, 67, 73, 93, 105, 112 and 125 were missing. This has now been corrected.